Thermographic stepwise assessment of impact damage in sandwich panels

Chiara Colombo[a], Mohamed Harhash[b], Heinz Palkowski[b], Laura Vergani[a,*]

[a] Politecnico di Milano, Department of Mechanical Engineering, Via La Masa 1, 20156 Milano, Italy
[b] Clausthal University of Technology, Institute of Metallurgy, Robert-Koch-Str. 42, 38678 Clausthal-Zellerfeld, Germany

Metal-polymer-metal sandwiches can find promising applications in the automotive field thanks to their lightweight and formability. The paper focuses on the effect of low velocity impacts on the residual mechanical behavior. Experimental stepwise tests are run on undamaged and impacted specimens with different combi-nations of thickness and grade for the outer steel skins and the inner polymeric core. Surface temperature evolution is thermally monitored during the tests with the aim to characterize the induced damage and to identify a parameter able to quantify the residual strength of the panel. Several approaches have been con-sidered. The analysis of the thermal amplitude trend with the lock-in thermography evidences a variation in the thermal behavior of the specimens, defining a corresponding damage stress σ_D. We found a 20% σ_D difference between undamaged and damaged specimens. Moreover, impacted specimens experience a temperature and stress concentration at the impact area dependent on the indentation.

Based on these results, we evidence the possibility to relate impact indentation with the damage stress estimated by thermography and with the stress concentration factor induced by the impact. Therefore, thermography is a useful and valid tool for post-impact damage detection, monitoring and quantification of these multilayer sandwich materials.

Keywords:
Sandwich panel, Impact, Thermography, Variable stress amplitude Damage stress

1. Introduction

The present work focuses on sandwich panels with a metal-polymer-metal (MPM) structure. These panels are designed for weight-reduction when compared to a full structure and have many interesting characteristics for the mechanical designer such as good formability [1] [2], good damping properties with low polymer thicknesses, grades and thicknesses customizable to special requirements, possibility of asymmetric structures, high bending and buckling stiffness, possibility to be welded as well as adhesively joined, and attractive costs [3].

These hybrid panels are thought for automotive applications (i.e. side and roof panels of cars, vans and coaches) thanks to their lightweight and formability. In this field, the use of these panels is recently becoming more and more popular. For instance, Litecor® is a sandwich developed within the project InCar® Plus by ThyssenKrupp [4] and it is applied to commercial cars and trucks for internal and external panels. Through this material, they claim a weight reduction of these structures up to 40%.

Low velocity impacts, as the case of stones or small objects against vehicle panels, are very frequent for these applications caused for instance by hailstorms or ballast, and they can typically generate well visible damaged regions with plastic strains. It is often not easy to evaluate the effect of these damages on the residual mechanical behavior of the panels and to identify threshold damages before panel removal.

The parameter that could be more easily measured is the extension of the impacted zone and in particular the dome depth. However, in order to quantify the damage induced by these impacts, it is important to relate the dome depth to the effective residual strength of the panel. With this aim, in a previous work [5] we tried to quantify the damage by means of thermographic measurements. Impacted MPM sandwich panels were subjected to static tensile tests and monitored by a thermal camera. The effect of the impact was evaluated by defining a stress of damage initiation σ_D on undamaged and impacted (i.e. at the dome) samples. It was found that the damage stress at the dome region was up to 11% smaller than the one of undamaged specimens, with some variability depending on the steel grade used for the skins.

In the present paper we propose different thermographic approaches to quantify the effective damage of an impacted panel with respect to the depth of the dome that is a parameter easily measurable.

In particular, we apply cyclic loads with variable stress amplitude (stepwise tests), thermally monitoring the surface temperature trend of the specimens with the aim to quantify the plastic-induced damage.

To obtain significant values, we follow different thermographic

Received 19 July 2017;
Received in revised form 11 September 2017;
Accepted 2 October 2017
Available online 04 October 2017

* Corresponding author.
E-mail address: laura.vergani@polimi.it (L. Vergani).

Published Journal Article available at: http://dx.doi.org/10.1016/j.compstruct.2017.10.001

techniques. We identify two parameters that seem able to quantify the induced damage: 1) the damage stress evaluated from the mean and amplitude temperature trend and 2) the stress concentration factor thermally evaluated. These parameters summarize the comparison of the thermal response between undamaged and impacted regions. In the literature, these approaches were extensively applied to homogeneous materials; as far as the authors know, they have not been applied to sandwich materials yet.

2. The sandwich panels

Object of this work are MPM panels, made of two metal skins and an inner polymeric core. Epoxy resin (Köratec 201) is used to bond the two metal sheets with the polymeric core. The manufacturing process of these MPM panels is based on a surface pre-treatment to activate this epoxy resin, followed by the roll bonding process between two steel cover sheets and the core made of a polyolefin foil, i.e. a blend of polypropylene and polyethylene (PP/PE) [6].

Different configurations with variable thickness are considered. These thickness variations of the metal sheets and the polymeric core are taken into account to evaluate the possibility to design a lightweight and customizable structure, able however to sustain loads and keep adequate stiffness.

Table 1 shows the types of sandwich panels tested in the present work. All these MPM panels present an inner core in polyolefin with variable thickness. Different steel grades of deep drawing qualities are selected in accordance with EN10027-1 standard with variable thickness. The identification of the panels in Table 1 reflects the thickness of the layers and the steel grade.

Table 2 reports the mechanical properties of the sandwich constituents and of the panels obtained from tensile static tests according to ISO 6892-1:2016. Values are averaged based on four tests. The values without tolerance range were calculated using the rule of mixtures. The applicability of this rule for calculating the mechanical properties of the panels was stated in [7] and [8].

Table 2
Mechanical properties from static tests.

Steel grade – Thickness (mm)	E (GPa)	YS (MPa)	UTS (MPa)
a. Sandwich constituents			
0.49 TS 245	180 ± 10	212 ± 7	319 ± 8
0.24 TS 245	170 ± 10	193 ± 5	281 ± 20
0.49 TH 470	194 ± 5	467 ± 21	514 ± 0.45
PP – PE	1.98 ± 0.2	28 ± 2	28 ± 2
b. Sandwich panels. Values without standard deviations are estimated by the rule of mixtures			
0.135/0.6/0.135 TH620	64 ± 2	193 ± 2	199 ± 2
0.135/1.2/0.135 TH620	35	114	114
0.49/0.6/0.49 TH470	99 ± 1	324 ± 6	326 ± 5
0.49/1.2/0.49 TH470	88	160	161
0.24/0.3/0.24 TS245	104 ± 5	138 ± 1	209 ± 1
0.24/0.6/0.24 TS245	70 ± 5	102 ± 1	158 ± 0.9
0.24/1.2/0.24 TS245	49	74	100
0.49/0.6/0.49 TS245	109 ± 15	135 ± 8	209 ± 9
0.49/1.2/0.49 TS245	82	110	158

3. Experimental setup, equipment and techniques

3.1. Impact tests

Impact tests are performed by a drop weigh tower, clamping the panels at the ground with a rigid frame. The guiding mechanism is a vertical pipe in polycarbonate. Some holes are drilled to avoid air compression. The impact free area is $60 \times 60\,mm^2$ (see Fig. 1a).

The impacting mass has a semi-spherical tip with diameter 25.4 mm; this tip was subjected to surface hardening, ensuring that during the test any damage occurs at the panel, and not in correspondence of the impactor tip. Above the tip, a load cell (Kistler 9331B) connected with a signal amplifier (Kistler 5011B) is placed, to record the impact time. The total impacting mass is 1.47 kg (see Fig. 1b).

The impact energy is evaluated from the impactor velocity. With this aim, two lasers (M7L/20 by Microlelectronics) are placed laterally on a support, very near to the panel, as shown in Fig. 1b.

Load cell and laser signals are collected by an acquisition card (NI9239 and NI cDAQ 9171 by National Instruments). Finally, impact data are handled by NI Signal Express 2015 software with an acquisition frequency set to 50 kHz and the impact velocity v_{impact} evaluated as:

$$v_{impact} = \frac{s_{laser}}{t_1 - t_2} + \left(t_3 - \frac{(t_1 + t_2)}{2}\right) \cdot g \quad (1)$$

where: s_{laser} is the vertical distance between the two lasers (20 mm), t_1 and t_2 are the times of impactor detection by the lasers, t_3 is the impact time recorded by the load cell and g is the gravity constant (see Fig. 1b). The resulting impact energy is 9.0 ± 0.4 J with an impact velocity equal to 3.51 ± 0.08 m/s.

Three over four 0.135/1.2/0.135 TH620 panels, thus with the thinnest steel layers, experienced a crack at the skin opposite to the impact. These panels are therefore discarded.

3.2. Measurement of impact indentation

After the impacts, two techniques are experimentally used to measure the indentation.

At first, the impact depth, i.e. the dome, is measured by photogrammetry (DIC), which is an optical technique evaluating the deformation of a grid pre-printed on the panel surface. Measuring the out-of-plane displacements on both panel sides by means of photogrammetry, the thickness reduction at the dome is also evaluated and resulted between 8% and 16% of the total initial thickness, depending on the thickness of the steel layer (see Fig. 2a).

The indentation measures are also repeated by a profilometer (Zeiss Prismo 5 VAST MPS HTGCMM, accuracy: 3 μm) as out-of-plane displacements along a straight line centered at the dome, only on the

Table 1
The sandwich panels.

Panel identification	Steel grade	Steel thickness [mm]	Polymer type	Polymer thickness [mm]
0.135/0.6/0.135 TH620	TH620	0.27	PP-PE	0.6
0.135/1.2/0.135 TH620	TH620	0.27	PP-PE	1.2
0.49/0.6/0.49 TH470	TH470	0.98	PP-PE	0.6
0.49/1.2/0.49 TH470	TH470	0.98	PP-PE	1.2
0.24/0.3/0.24 TS245	TS245	0.48	PP-PE	0.3
0.24/0.6/0.24 TS245	TS245	0.48	PP-PE	0.6
0.24/1.2/0.24 TS245	TS245	0.48	PP-PE	1.2
0.49/0.6/0.49 TS245	TS245	0.98	PP-PE	0.6
0.49/1.2/0.49 TS245	TS245	0.98	PP-PE	1.2

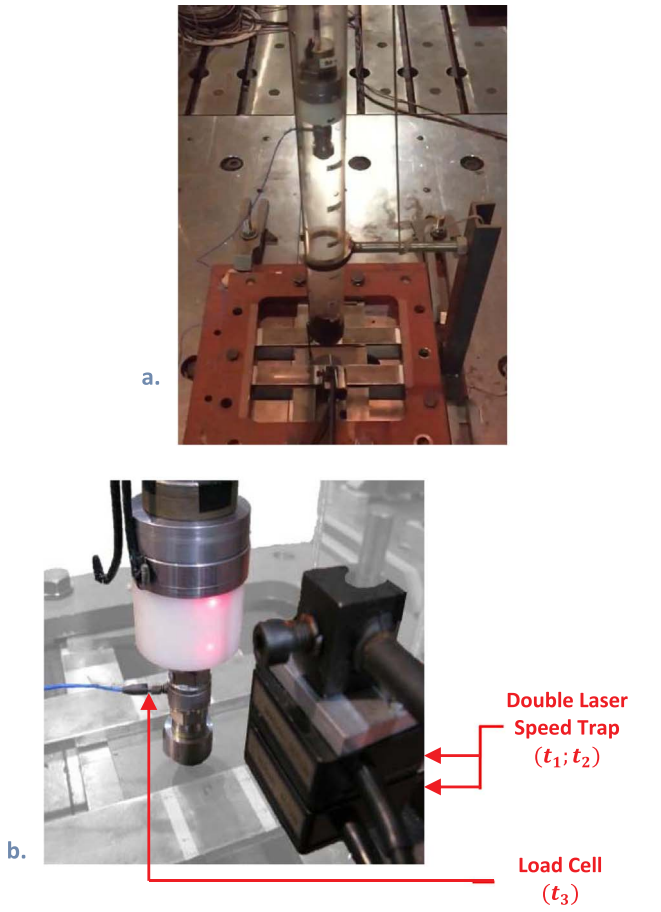

Fig. 1. Setup for experimental testing: a. drop weight tower and b. detail of the impactor.

impact side. This allows to create a 2D profile of the impact. Since after the impact the panels are deformed and curved, the indentation measure with the profilometer has not a reference plane. For this reason, we set as reference for the indentation measure a distance (left and right sides) of 12.7 mm from the deepest point, i.e. having the minimum out-of-plane displacement. This region corresponds to the size of the impactor tip.

The indentation of the profilometer is a relative measure and it is smaller than the indentation evaluated by photogrammetry, due to the fixed reference plane. Indeed, data obtained by photogrammetry range from 0.6 to 4 mm; data obtained by the profilometer range from 0.6 to 2.5 mm. Fig. 2b compares these indentations measured by the photogrammetry and by the profilometer; data are least squared interpolated with a straight line, evidencing a good agreement between the two methods.

Based on this comparison, we can estimate that the measure on the impact side is sufficient to describe the impact effect, without considering also the variation in thickness. Moreover, the two measures of the dome by photogrammetry and by the profilometer give similar results. For this reason, in the following of the paper we consider as impact depth the results obtained from the profilometer, which is easier to be performed not only on the samples but also on real impacted structures.

3.3. Post-impact stepwise tests

After impacting the panels, rectangular strips 45 × 200 mm^2 are cut with a saw. The impact region was centered in the specimen. In addition, undamaged specimens with hourglass shape are prepared by a CNC milling machine (Fig. 3).

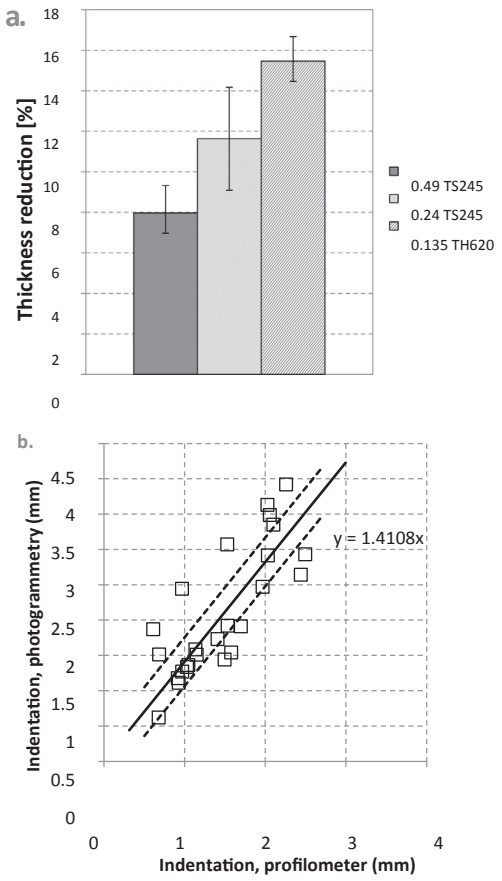

Fig. 2. a. Thickness reduction of the sandwich panels as a function of the thickness of the steel layer; b. comparison between data from photogrammetry and profilometer (all available data): the solid line is the least square linear interpolation and the dashed lines are the upper and lower confidence bands at 99.5% probability.

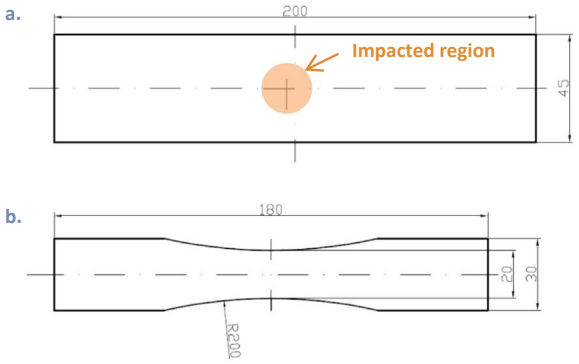

Fig. 3. Dimensions of the specimens in mm: a. damaged; b. undamaged.

The stepwise tests are performed in load control, applying loading blocks at different stress amplitudes $\Delta\sigma$ with a stress ratio $R = 0.1$ and a loading frequency $f_L = 20$ Hz. Each block lasts 1000 cycles. The testing machine is a uniaxial servo-hydraulic MTS Landmark equipped with a 100 kN load cell.

The surface temperature is monitored by an infrared (IR) thermal camera, type FLIR Titanium SC7000, placed at a distance of around 300 mm from the specimen surface. The thermal sensitivity of the camera is up to 20 mK; the spatial resolution is 320 × 256 pixels. The frequency of thermal sampling f_S is set to 50 Hz.

All the specimens are sprayed with a thin layer of black matt paint, to provide an enhanced and uniform surface emissivity and facilitate thermographic measurements. Before starting the tests, the thermal

camera measurement is calibrated with a black body (non-uniformity compensation, NUC).

3.4. Thermo-elasticity and Lock-in thermography

When a body is subjected to cyclic load, it experiences a resultant cyclic temperature field characterized by different frequencies. In the literature, the fundamental thermoelastic relationship between applied stress and reversible thermal response was first introduced by Lord Kelvin [9] for homogeneous materials in adiabatic conditions, i.e. relating the elastic variation in volume of the loaded body with the surface temperature, through a thermoelastic constant. The work by Wong et al. [10] pointed out that this thermoelastic constant is actually a function of the mean applied stress, by introducing the dependence of the elastic properties with the temperature (i.e. dE/dT). More recently, mainly due to the evolution and improvements in the thermal sensors, thermoelastic stress analysis [11] [12], Lock-in thermography [13] [14], and Lock-in dissipative thermography [15] [16] were developed.

Focusing on this last thermographic technique, the surface temperature of the object is recorded by an infrared camera and compared with the excitation signal: indeed, Lock-in thermography is also called modulated thermography. Fig.4 presents a simplified scheme of the mechanical input and thermal output during the stepwise tests. Other low and high frequency noisy components can be present, but they will not be considered, as they are typically filtered.

During the mechanical testing and thermal monitoring performed in the present work, the considered input signal for the thermal processing (reference signal) is the mechanical load cell sinewave. This signal is transformed in voltage (0–5 V) by the software of the testing machine and connected with a BNC cable to the Lock-in module of the thermal camera. No strain gauge is glued to the surface, to avoid that any local heat source could influence the global surface temperature.

The test output is the IR monitored surface temperature of the specimen. By means of the Lock-in module, this signal can be decomposed in two parts through a Fast Fourier Transform: the signal having the same frequency of the mechanical input f_L and the signals with different frequencies, typically higher when plasticity occurs. They correspond respectively to the thermoelasticity or E-mode (Emission Mode) and to the D-mode (Dissipation Mode), according to Altair LI software by Flir®, which has been used in the present work. In brief, E-mode analyzes the first order harmonic (principal harmonic) and it is related to the theory of the thermoelastic effect and of the thermoelastic stress analysis. On the other hand, D-mode considers the second harmonic signal. The literature evidenced the importance of this dissipative signal with many applications. For instance, [14] is one of the first works correlating the presence of dissipation effects to the increase of the second harmonic signal amplitude; that paper proposed a study on the self-heating and the dissipated energy accompanying the high cycle fatigue of a dual-phase steel grade. [17] showed how the second harmonic can be used to detect both cracking and delamination damage in composite structures. In [18], the dissipation mode was applied to the detection of damage initiation in basalt reinforced plastics. Moreover, the authors of [19] proposed the analysis of the second harmonic as a promising approach to detect the load amplitude threshold at which dissipative damage phenomena start occurring in a natural flax fiber reinforced epoxy polymer composite. Therefore, it resulted that the dissipation mode can be interesting not only for the study of damage in homogeneous materials but also for composites.

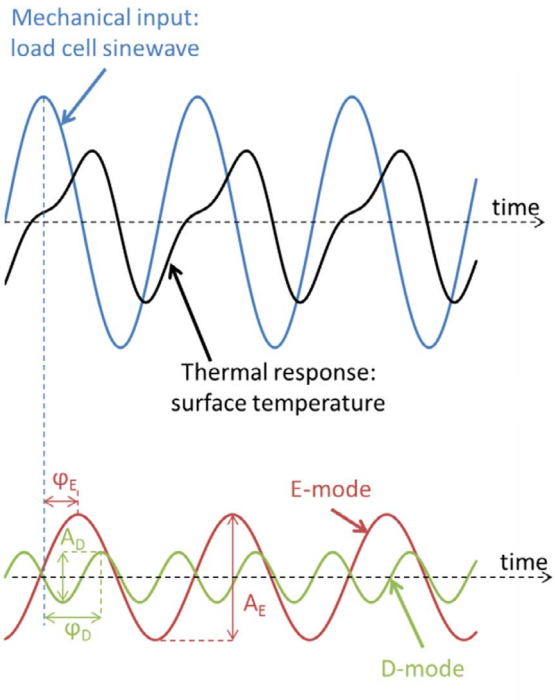

Fig. 4. Simplified scheme of mechanical and thermal signals.

Each one of these two signals, first and second harmonic, can be analyzed in terms of amplitude A and phase ϕ (see schematics in Fig. 4) [20].

The thermoelastic amplitude A_E increases linearly with the applied $\Delta\sigma$, which is the first stress invariant. This means that the elastic stress field changes with $\Delta\sigma$ in a homothetic way and the overall stress range remains representative of the stress pattern. The thermoelastic linear law, valid for homogenous materials, is given by [9]:

$$\Delta T = -K_m \cdot T_{mean} \cdot \Delta(\sigma_x + \sigma_y) \tag{2}$$

where the thermoelastic constant K_m directly relates to the temperature amplitude ΔT with the in-plane stress variation. Considering that the thermal monitored surface, that is the external skin of the MPM, is made of steel, the validity of Eq. (2) can be extended to the present analysis of the sandwich, allowing to relate the thermal measurements with the surface state of stress in the panels. A detailed description in energy terms is given in [21].

When the applied load increases, plasticity develops inducing a stress redistribution. Therefore, the presence of a stress concentration may explain why the thermoelastic amplitude is no longer proportional to $\Delta\sigma$. In this condition, Eq. (2) is not more valid and the thermoelasticity has no longer physical sense. The loss of linearity is naturally less important in regions where the stress gradients are softer.

Focusing on stepwise cycling, different thermographic techniques can be applied to the experimental analysis of thermal data. These techniques can consider the trends of mean temperature or of temperature amplitude. Both of them aim identifying a stress of damage initiation σ_D into the considered structure, based on the IR-thermographic data. This σ_D, which can be considered as a limit stress, corresponds to the deviation from the initial linear trend, or, in other words, it should identify the change in the thermal response of the sample before any damage occurs.

4. Thermographic analysis

4.1. Analysis of the mean temperature

The studies by [15] and [22] on homogeneous materials identified thermographically a stress connected to the damage initiation, detected from the bi-linear curve of the temperature gradient over the cycles and the applied maximum stress (i.e. $\Delta T/\Delta N$ vs σ_{max}). This method was applied also to composite materials, obtaining interesting results in [18] and [23]. In the present work we aim to extend the validity of this technique to the damage detection of the undamaged and impacted sandwich panels.

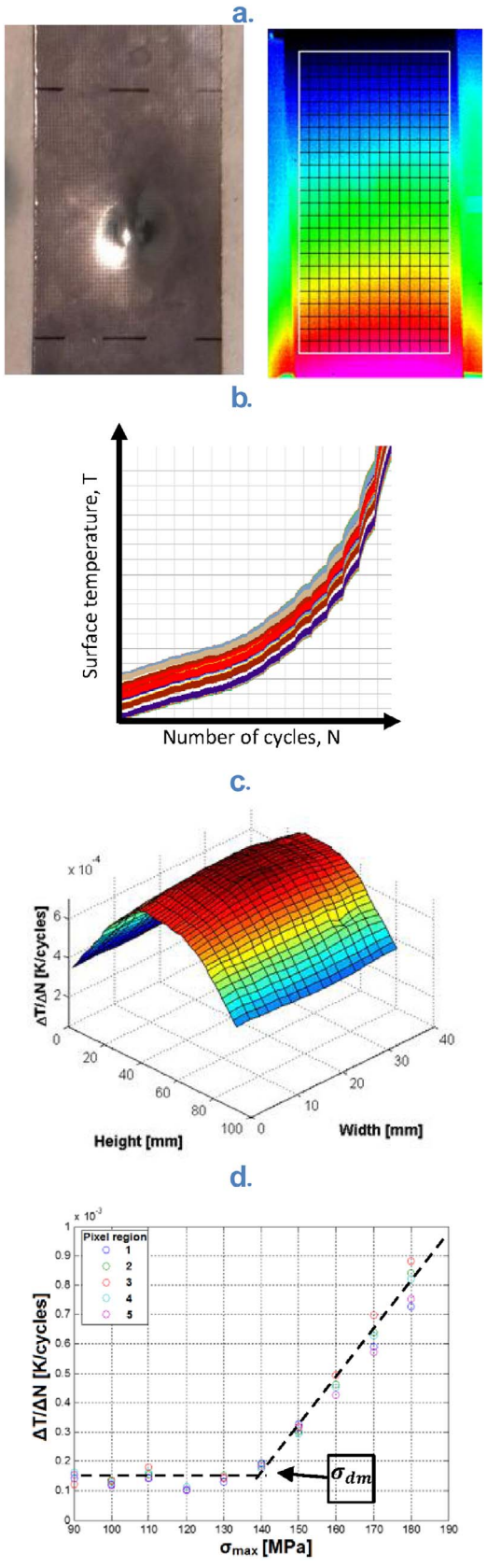

Fig. 5. Steps for thermal data analysis and identification of σ_{Dm}: a. Real specimen before spraying and grid generation on thermal data; b. thermal data extraction (Temperature vs cycles); c. plot of $\Delta T/\Delta N$ over specimen surface, for each load step; d. plot of $\Delta T/\Delta N$ vs σ_{max} and identification of σ_{Dm} for different areas. These areas correspond to: 1: dome; 2–5: up, down, left and right sides.

Fig. 5 shows the procedure followed to identify the damage stress σ_{Dm} from the mean temperature trend:

1) the thermal maps of specimen surfaces are sub-divided with a grid of 5×5 pixels, corresponding to $2 \times 2\,mm^2$;
2) (Fig. 5a). Indeed, considering each single pixel would result in a high noise on the thermal signal, thus useless for the following analysis;
3) for each one of these squared regions, the thermal history is extracted and averaged over the area, as a function of the number of cycles (Fig. 5b);
4) for each loading step, a temperature gradient $\Delta T/\Delta N$ is extracted, calculated from the initial linear trend, and therefore obtaining a 3D thermal map (Fig. 5c) over the surface of the specimen;
5) thermal gradients $\Delta T/\Delta N$ are finally plotted as a function of the maximum applied stress σ_{max}, obtaining different bilinear curves, one for each pixel region (Fig. 5d).

This procedure is implemented in a Matlab® script and run for each specimen to obtain the corresponding σ_{Dm} value in each squared region. All the impacted specimens experienced a region, central and near to the dome, where the temperature reaches higher absolute values (Fig. 5c). However, plotting the surface temperature T vs the number of cycles N is only shifted and the trends for all the regions are similar. The behavior is evidenced in Fig. 5b, and confirmed in Fig. 5d, that there is no evidence of a difference in σ_{Dm} estimation for all these regions. Therefore, this method seems not able to identify the damage introduced into the sandwich by the impact. For each panel type, in fact, the damage stress σ_{Dm} results similar between undamaged and impacted panels. Therefore, it seems that, for this sandwich, the analysis of the mean temperature in terms of $\Delta T/\Delta N$ catches only a more general behavior of the material, not specific of the impact damage.

For sake of completeness, it must be mentioned that the σ_{Dm} determination is possible only for sandwich panels having more ductile behavior (i.e.TS245 steel). For all other tested steel skins with a more brittle behavior (TH470 and TH620 steels), the change in thermal response is really near to failure and an estimation of σ_{Dm} results near to the YS and UTS. For this reason, the results we propose are related only to TS245 steel sandwich.

Fig. 6 summarizes σ_{Dm} estimations for TS245 steel skins, combining the indentation measurements from the profilometer. Due to the wide data scatter, the fitting is not meaningful and it seems that σ_{Dm} for undamaged and impacted specimens is very similar. The low performances of the mean temperature method with MPM materials, discussed in the present paragraph, could be a consequence of the complex through-the-thickness heat conduction that can be altered by the bi-

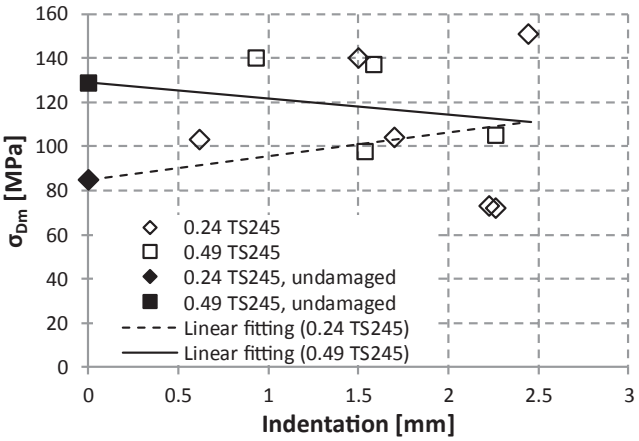

Fig. 6. Damage stress σ_{Dm}, evaluated from mean temperature trend, as a function of indentation measurements from profilometer.

material non-homogeneity at the meso-scale. The metallic and polymer layers have very different thermal properties in terms of heat conduction and heat capacity, and this may alter the trend of the mean temperature regardless of the local or extended level of damage achieved by the materials.

4.2. Analysis of the thermoelastic signal

In this section we apply the concepts described in 3.4 based on the Lock-in thermography. We analyzed with Altair LI software by Flir® the temperature amplitudes and phases of 1) the signal having the same frequency of the mechanical input by thermoelastic stress analysis (TSA) and 2) of the second harmonic signal by the dissipation mode. After analyzing all these data, we found that, for the panels object of this work, the thermoelastic amplitude is the most suitable variable to be monitored, while from the TSA in terms of phase shift, and from the dissipation mode in terms of both module and phase, no specific information is found to identify the presence of the dome. In particular, the phase was uniform over all the analyzed areas, thus confirming the adiabaticity of the test. Hence, results and comments are proposed only for the analysis of the thermoelastic signal, with the aim of quantifying the damage located at the impact dome.

4.2.1. Thermoelastic signal vs maximum applied stress

An interesting and promising way for analyzing the thermographic data is suggested by plotting the trend of the module of the thermoelastic signal as a function of the maximum applied stress σ_{max} progressively increased during the stepwise fatigue cycling. This maximum stress, σ_{max}, is a nominal value calculated by considering the maximum applied load divided by the total area of the panel.

Fig. 7 shows the thermoelastic signal history for a tested specimen (0.24/1.2/0.24 TS245), for three main instants: 1) the elastic stage, 2) the damaging stage, 3) the final failure. For small loads, this temperature field analyzed by thermoelasticity is proportional to the stress field through Eq. (2). Since the beginning of the test, an increase of temperature is evident at the impact region.

Analyzing the 5 × 5 pixel region with the highest thermoelastic signal (i.e. at the sides of the dome), we obtained a trend of these signals during the test. Fig. 8 shows this trend for an impacted specimen 0.24/1.2/0.24 TS245. This trend can be divided in three regions:

1) region 1: an initial linear trend between the module of the thermoelastic signal and σ_{max}, related to the thermoelastic behavior of Eq. (2);
2) region 2: a flat central region, where the thermoelastic signal is constant even increasing the applied load;

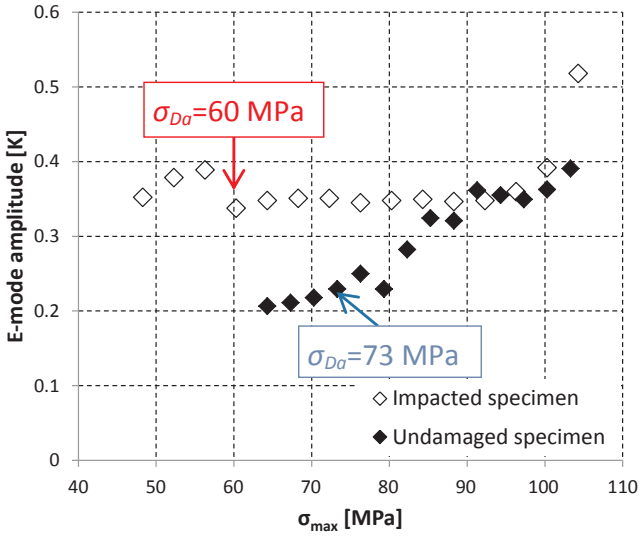

Fig. 8. Trend of the thermoelastic signal as a function of the applied stress for each loading step in an undamaged and an impacted 0.24/1.2/0.24 TS245 specimen. Identification of the damage stress σ_{Da}.

3) region 3: a final and quick increasing of the thermoelastic signal in the last step identifying failure.

Different areas were selected on the monitored surfaces of the specimens. The local value of the thermoelastic signal module changes, but always experiencing an alteration at the same stress level. Therefore, it seems that, at a certain load level (i.e. corresponding to σ_{Da}, that is the damage stress evaluated from the amplitude trend of the surface temperature), there is a common and spreading damage into the panel. Based on this experimental observation, we define σ_{Da} as the upper limit of the thermoelastic region (end of region 1).

This behavior is less visible in the undamaged specimen also plotted in Fig. 8. Only two main regions are present in this case: an initial trend with a very small slope, followed by an increase of the thermoelastic signal. At the end of the initial linear stage, σ_{Da} can be identified also for these undamaged samples.

At the end of the stepwise test, the undamaged and impacted specimens experience a similar behavior of the thermoelastic signal and the trend is almost overlapped (Fig. 8: $\sigma_{max} > 90$ MPa), thus meaning that in this high-load region the effect of the impact is no more appreciated.

It should be mentioned that also the sandwich panel with more

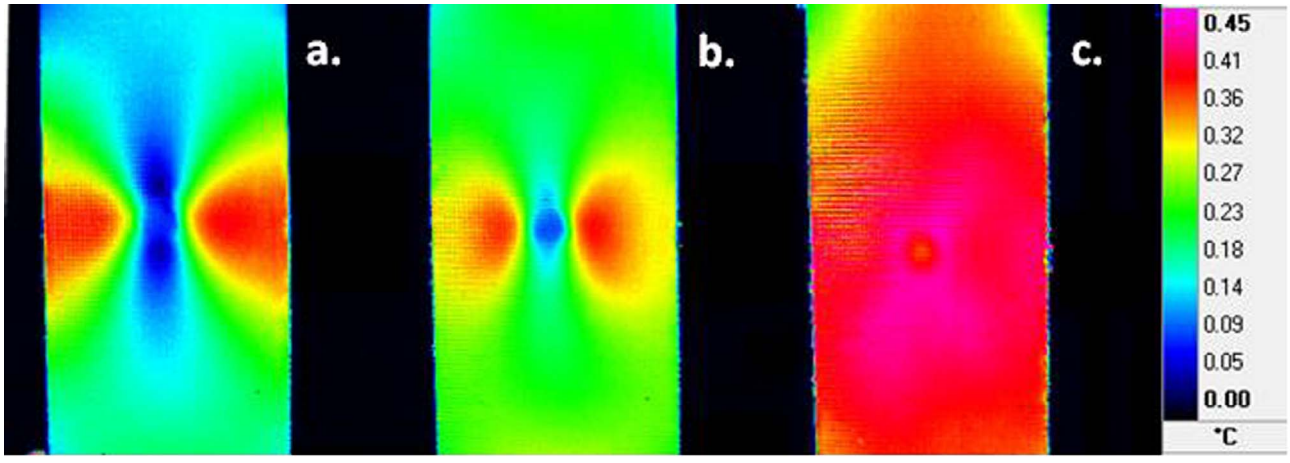

Fig. 7. Thermoelastic signal: a. loading step in the elastic regime, $\sigma_{max} = 52$ MPa $< \sigma_{Da}$; b. loading step in the progressive damage regime, $\sigma_{max} = 76$ MPa $> \sigma_{Da}$; c. last step before final failure $\sigma_{max} = 100$ MPa.

Table 3
Estimation of σ_{Da} from E-mode module.

Panel type	σ_{Da} damaged [MPa]	σ_{Da} undamaged [MPa]	Difference%	Impact depth [mm]
0.24/1.2/0.24 TS245	63	77	23%	2.2 mm
0.49/0.6/0.49 TS245	140	180	29%	0.9 mm
0.49/1.2/0.49 TS245	111	135	22%	1.5 mm
0.49/1.2/0.49 TH470	220	230	4.5%	0.9 mm

brittle skins experiences this trend, even if regions 2 and 3 are very near to failure, thus resulting in a σ_{Da} close to the UTS of the sandwich. Table 3 reports the σ_{Da} estimations of different sandwich specimens. Specimens with the same type of external skins show a very similar decrease of σ_{Da} when compared with undamaged specimens, higher than 20%. On the other hand, TH470 steel has a very limited variation, smaller than 5%. Hence, this more brittle steel seems less prone to be influenced by impacts.

Fig. 9 shows the trend of this damage stress σ_{Da} as a function of the impact depth of the TS245 steel skin. Three different MPM panels are considered in the graph, with skins of 0.24 and 0.49 mm. The lowest values of σ_{Da} are estimated for the panels with 0.24 mm skins. The use of a double thick core layer for the panels with 0.49 mm skins seems slightly decreasing the overall mechanical property after the impact.

4.2.2. Thermoelastic signal and definition of a temperature concentration factor, K_t

Stepwise tests on non-damaged specimens allow for the estimation of the thermoelastic constant K_m for $\sigma_{max} < \sigma_{Da}$, based on Eq. (2). Several tests confirm this relationship until reaching a certain threshold ΔT_{th} (see Fig. 10). Indeed, up to this temperature value, the stress-temperature relationship is linear and the thermoelastic theory is applicable. Table 4 reports the estimations of K_m, which are near to the typical values of steels reported in the literature ($K_m = 3.5{\cdot}10^{-6}$ 1/MPa [12]). Once K_m is estimated, the surface state of stress for the impacted panels is also determined from the surface temperature.

Recalling the thermoelastic signal history of Fig. 7, We can also observe that the plastic region creates a local increase, and therefore a stress concentration, similar to the case of a plate with a hole subjected to tensile load. This "temperature concentration" is evident from the initial loading steps (Fig. 7a), while the effect decreases overcoming σ_{Da} (Fig. 7b). Near to failure, the field of the temperature amplitude increases and it is almost uniform on the surface of the specimen (Fig. 7c). Based on this experimental observation, a stress concentration factor K_t

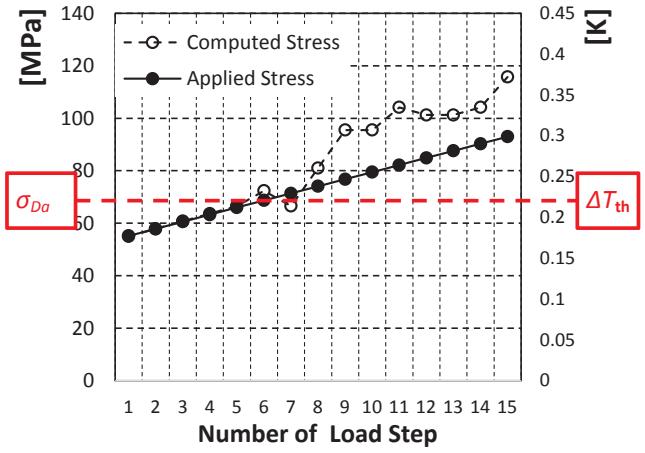

Fig. 10. Limit of applicability of Eq. (2): analysis on the undamaged specimen 0.24/1.2/0.24 TS245: identification of the temperature threshold ΔT_{th}.

Table 4
Evaluated stress concentration factors.

Panel type	K_m [1/MPa], from undamaged specimens	Average stress concentration factor, K_t	Average impact depth [mm]
0.24/1.2/0.24 TS245	$1.14{\cdot}10^{-5}$	2.0	2.24 mm
0.49/1.2/0.49 TS245	$7.21{\cdot}10^{-6}$	1.6	1.47 mm
0.49/0.6/0.49 TH470	$7.85{\cdot}10^{-6}$	1.7	1.14 mm
0.49/1.2/0.49 TH470	$4.53{\cdot}10^{-6}$	1.2	0.97 mm

can be identified for each impacted panel as the ratio between maximum and nominal temperature:

$$K_t = \frac{\Delta\sigma_{max}}{\Delta\sigma_{nom}} = \frac{\Delta T_{max}}{\Delta T_{nom}} \tag{3}$$

In order to experimentally determine the concentration factor K_t, we use the following procedure:

1) on undamaged specimens and from the initial loading steps with $\sigma_{max} < \sigma_{Da}$, performed at a given applied stress amplitude $\Delta\sigma_{nom}$, Eq. (2) allows estimating the related nominal temperature amplitude ΔT_{nom};
2) on impacted specimens and at the same loading stress (with

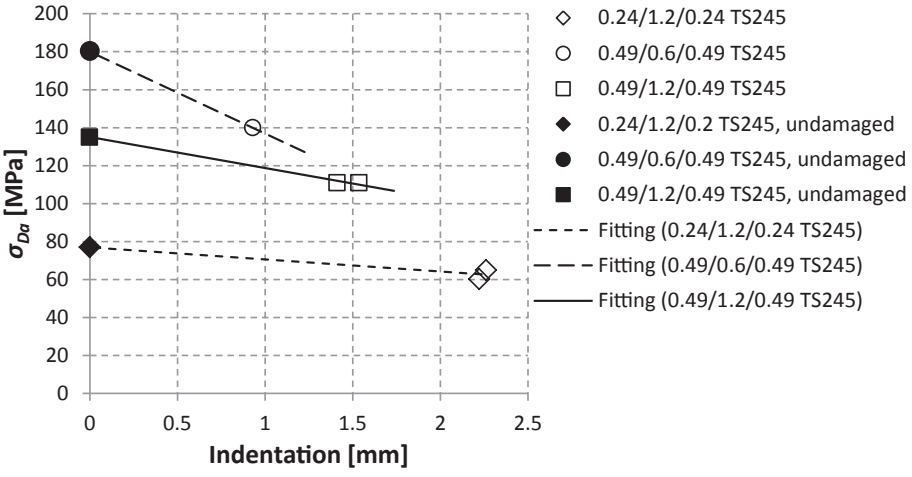

Fig. 9. Damage stress σ_{Da}, evaluated from the thermoelastic signal, as a function of indentation measurements by the profilometer.

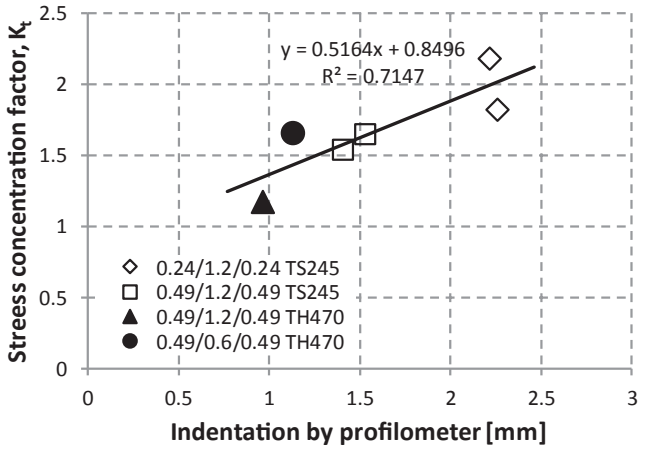

Fig. 11. Measures of stress concentration factor, K_t, as a function of the impact indentation measured by profilometer.

$\sigma_{max} < \sigma_{Da}$ as in Fig. 7a), the maximum temperature amplitude ΔT_{max} is evaluated experimentally as the recorded peak temperature from the thermoelastic signal, which is located at the sides of the impacted region;

3) K_t is estimated from Eq. (3).

Table 4 shows the resulting stress concentration factor (or temperature concentration factor) K_t for some analyzed types of panels. From these results it appears that K_t increases with the depth of impact indentation. Moreover, K_t is not affected by the material properties, but the only dependence is on the damage induced by the impact, thus the indentation.

This concept is also shown in Fig. 11, where a unique regression line is plotted for all the different types of panels. When a given impact indentation is experimentally measured on the panels, an equivalent K_t can be estimated through this curve. Based on this consideration, K_t can be estimated as a temperature concentration factor and it could result a useful thermographic parameter for the estimation of the damage effect.

5. Conclusions

This paper presented a study on the impact damage of metal-polymer-metal (MPM) sandwich panels for automotive applications. Thermography is the experimental technique here proposed to quantify this damage. The study aimed to identify a limit stress, called damage stress σ_D, and to correlate it with the impact indentation, i.e. the out-of-plane displacement of the panel. Experimental stepwise fatigue tests carried out on impacted and undamaged specimens were thermally monitored. Thermal data were analyzed in terms of average temperature trend and thermoelastic signal. Some final considerations can be drawn for this sandwich material:

- by means of the average trend of the temperature, it was possible to evidence a change in the average thermal answer and to obtain the damage stress σ_{Dm} of the sandwich. No variation due to the impact could be evidenced;
- by means of the thermoelastic signal, we could identify a three-linear trend (increasing-flat-increasing) of this signal as a function of the maximum applied stress. We identified both for undamaged and impacted specimens σ_{Da} as the stress at the end of the initial stage. σ_{Da} for undamaged specimens are always higher than for impacted ones. Crossing the results of σ_{Da} stresses, it was evidenced that specimens with more ductile skins (TS245) show approximately 20% decrease in σ_{Da} when compared with undamaged specimens, independently on the different thickness of the steel skins or the polyolefin core. Specimens with more brittle skins (TH470) experienced only a 5% variation, underlying that this more brittle steel seems less prone to be influenced by impacts.
- finally, further analyzing this thermal amplitude during cycling, we could identify a temperature intensification at the dome. This allowed defining a temperature concentration factor, proportional to the stress concentration factor K_t. This parameter increases with the panel indentation and is independent on the sandwich steel and total thickness. This parameter seems to well summarize the effect of the impact damage on the panel.

Based on these considerations, we can claim that the use of thermography, and in particular the analysis of the thermal amplitude, can give interesting information on the state of damage of these impacted MPM sandwich panels. More in details, we proved that it is possible to relate the measure of the impact dome with the stress and temperature concentration and finally with the damage stress. This measure can be useful for designers to evaluate the residual strength and life of the impacted panels.

The results presented in this paper are preliminary data, which allow describing a procedure to quantify the damage induced by the impact through thermographic analysis. Further data will be developed to support this methodology applied to MPM sandwich panels.

References

[1] Sokolova OA, Carradò A, Palkowski H. Metal-polymer-metal sandwiches with local metal reinforcements: a study on formability by deep drawing and bending. Compos Struct Dec 2011;94(1):1–7. http://dx.doi.org/10.1016/j.compstruct.2011.08.013.

[2] Carradò A, Faerber J, Niemeyer S, Ziegmann G, Palkowski H. Metal/polymer/metal hybrid systems: towards potential formability applications. Compos Struct Jan 2011;93(2):715–21. http://dx.doi.org/10.1016/j.compstruct.2010.07.016.

[3] Burchitz I, Boesenkool R, van der Zwaag S, Tassoul M. Highlights of designing with Hylite – a new material concept. Mater Des 2005;26(4):271–9. http://dx.doi.org/10.1016/j.matdes.2004.06.021.

[4] ATZ extra. Application potential of Litecor in the body. In Alexander Heintzel, editor, The project ThyssenKrupp InCar Plus – Solutions for Automative Efficiency, pages 108–111. Springer Vieweg, 2014. URL https://incarplus.thyssenkrupp.com/navigator_atz_pdf_en/ATZ_InCar_plus_body_Litecor_potential_analysis.pdf.

[5] Colombo C, Carradò A, Palkowski H, Vergani L. Impact behaviour of 3-layered metal-polymer-metal sandwich panels. Compos Struct Dec 2015;133:140–7. http://dx.doi.org/10.1016/j.compstruct.2015.07.078.

[6] Carradò A, Sokolova O, Donnio B, Palkowski H. Influence of corona treatment on adhesion and mechanical properties in metal/polymer/metal systems. J Appl Polym Sci Feb 2011;120(6):3709–15. http://dx.doi.org/10.1002/app.33583.

[7] Harhash M, Carradò A, Palkowski H. Forming Limit Diagram of Steel/Polymer/Steel Sandwich Systems for the Automotive Industry. Springer International Publishing978-3-319-48096-1; 2016. http://dx.doi.org/10.1007/978-3-319-48096-1_20. 243-254.

[8] Harhash M, Carradò A, Palkowski H. Lightweight titanium/polymer/titanium sandwich sheet for technical and biomedical application. Materialwiss Werkstofftech 2014;45:1084–91. http://dx.doi.org/10.1002/mawe.201400356.

[9] Thomson (Lord Kelvin) W. On the thermoelastic, thermomagnetic, and pyroelectric properties of matter. Phil Mag Jan 1878;5(28):4–27. http://dx.doi.org/10.1080/14786447808639378.

[10] Wong AK, Jones R, Sparrow JG. Thermoelastic constant of thermoelastic parameter? J Phys Chem Solids Jan 1987;48(8):749–53. http://dx.doi.org/10.1016/0022-3697(87)90071-0.

[11] Pitarresi G, Patterson EA. A review of the general theory of thermoelastic stress analysis. J Strain Anal Eng Des Jan 2003;38(5):405–17. http://dx.doi.org/10.1243/03093240360713469.

[12] Greene RJ, Patterson EA, Rowlands RE. Springer handbook of experimental solid mechanics. Thermoelastic Stress Analysis. US: Springer; 2008. http://dx.doi.org/10.1007/978-0-387-30877-7. pp. 743–767.

[13] J.C. Krapez, G. Gardette, D. Balageas. Lock-in IR thermography: advantages and problems of some approaches. In Proceedings 3rd international workshop on advanced infrared technologies and applications, CAPRI; 19–20 September 1995, also published as ONERA TP 1995–153, 1995.

[14] P. Bremond, P. Potet. Lock-in thermography: a tool to analyze and locate thermo-mechanical mechanisms in materials and structures. In Andres E. Rozlosnik and Ralph B. Dinwiddie, editors, Thermosense XXIII. SPIE, Mar 2001. doi: 10.1117/12.421039.

[15] Luong MP. Fatigue limit evaluation of metals using an infrared thermographic technique. Mech Mater Jul 1998;28(1–4):155–63. http://dx.doi.org/10.1016/S0167-6636(97)00047-1.

[16] Ummenhofer T, Medgenberg J. On the use of infrared thermography for the analysis of fatigue damage processes in welded joints. Int J Fatigue Jan 2009;31(1):130–7. http://dx.doi.org/10.1016/j.ijfatigue.2008.04.005.

[17] Paynter RJH, Dutton AG. The use of a second harmonic correlation to detect damage in composite structures using thermoelastic stress measurements. Strain May 2003;39(2):73–8. http://dx.doi.org/10.1046/j.1475-1305.2003.00056.x.
[18] Colombo C, Vergani L, Burman M. Static and fatigue characterisation of new basalt fibre reinforced composites. Compos Struct Feb 2012;94(3):1165–74. http://dx.doi.org/10.1016/j.compstruct.2011.10.007.
[19] Pitarresi G, Tumino D, Mancuso A. Thermo-mechanical behaviour of flax-fibre reinforced epoxy laminates for industrial applications. Materials Nov 2015;8(11):7371–88. http://dx.doi.org/10.3390/ma8115384.
[20] Usamentiaga R, Venegas P, Guerediaga J, Vega L, Molleda J, Bulnes FG. Infrared thermography for temperature measurement and non-destructive testing. *Sensors* (Basel) Jul 2014;14(7):12305–48. http://dx.doi.org/10.3390/s140712305.
[21] Berthel B, Wattrisse B, Chrysochoos A, Galtier A. Thermographic analysis of fatigue dissipation properties of steel sheets. Strain Aug 2007;43(3):273–9. http://dx.doi.org/10.1111/j.1475-1305.2007.00349.x.
[22] La Rosa G, Risitano A. Thermographic methodology for rapid determination of the fatigue limit of materials and mechanical components. Int J Fatigue Jan 2000;22(1):65–73. http://dx.doi.org/10.1016/S0142-1123(99)00088-2.
[23] Vergani L, Colombo C, Libonati F. A review of thermographic techniques for damage investigation in composites. 1971-89932014;27:1–12. http://dx.doi.org/10.3221/IGF-ESIS.27.01.